Numerical Simulation of a Free Molecular Electro Jet (FMEJ) for In-Space Propulsion

Ariel Blanco[I] and Subrata Roy[II]
Applied Physics Research Group, University of Florida, Gainesville, FL, 32611

A design of a new class of plasma-based micro-thrusters is being proposed for in-space propulsion. This device, called Free Molecular Electro Jet (FMEJ), utilizes micro-actuators to accelerate the flow in a micro-channel with rarified gas. Numerical modeling of this device is being performed in order to predict the nature of the flow inside a micro-channel and the effectiveness of actuators for the given application. The numerical model is used to assess the improvements over existing micro-thruster designs such as free molecular micro resistojets and anode layer Hall thrusters. A finite element based multiscale ionized gas (MIG) flow code utilizing the Galerkin weak statement algorithm combined with an artificial diffusion method called Sub Grid eMbedding (SGM), is used to model the thruster using continuum approach. The results show that the thrust, specific impulse and efficiency seem to be similar to other electrical propulsion devices with similar input power despite the simplicity of the micro-thruster design.

Nomenclature

Kn	=	Knudsen number
L	=	physical length scale
λ	=	mean free path
k_B	=	Boltzmann constant
T	=	temperature
P	=	pressure
ρ	=	density
d	=	atomic diameter
a	=	atomic radius
n	=	number density
u	=	velocity in the x direction
v	=	velocity in the y direction
ν	=	collision frequency
α	=	recombination coefficient
S	=	ionization/recombination rate
m	=	molecular mass
ϕ	=	potential
ε	=	permittivity of free space
E_i	=	first ionization of Xenon
Z	=	charge state
φ	=	normalized ion production cost
C_v	=	specific heat at constant volume
C_p	=	specific heat at constant pressure
R	=	gas constant
κ	=	thermal conductivity
μ	=	viscosity
$\sigma_{v,T}$	=	momentum/thermal accommodation coefficient
$\dot{m}$	=	mass flow rate
F_{thrust}	=	thrust
I_{sp}	=	specific impulse

[I] Graduate Student, Mechanical and Aerospace Engineering, blanco07@ufl.edu, AIAA Student Member.
[II] Associate Professor, Mechanical and Aerospace Engineering, roy@ufl.edu, AIAA Associate Fellow.

I. Introduction

The Free Molecular Electro Jet (FMEJ) is a new class of electric micro-thrusters for microsatellites, with wide array of applications ranging from attitude control to drag compensation.[1] This class of thrusters aims to provide a means to impart milli-Newton-seconds of impulse while keeping the mass flow rate to a minimum. The FMEJ is a proposed improvement over the existing Free Molecular Micro Resistojet (FMMR), [2] which is an electro-thermal class of thruster. The proposed FMEJ design incorporates electro-hydro-dynamic flow acceleration techniques to increase the efficiency of the energy transfer from the electrical source to the propellant. Moreover, the presence of charged particles implies that both electric and magnetic fields can be used to produce the desired effect. In the past, studies have been conducted for plasma thrusters using DSMC.[3] However, no studies have been conducted based on micro-thrusters that use plasma actuators to accelerate the flow in the given flow regime to the best of our knowledge.

The basic idea behind the FMEJ concept involves embedding electrodes with an electric potential difference along the dielectric surface of the channel walls to produce a charged particle mixture called plasma. The directional nature of these charged particles as driven by the electric field can be used to impart collisional momentum to the propellant in the desired direction by appropriate design and placement of the electrodes. Figure 1 shows a schematic of one of the several possible arrangement of the device to explain the concept.

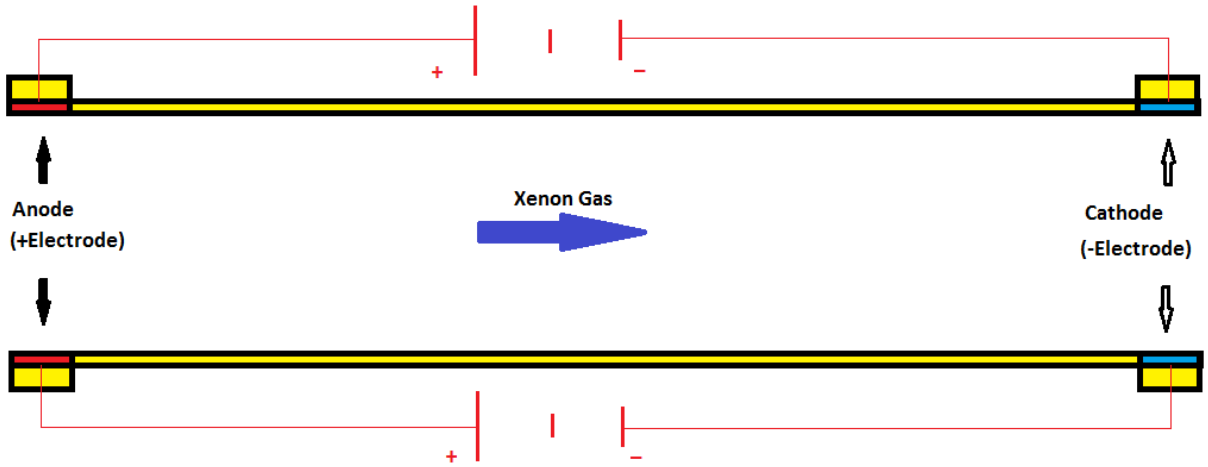

Figure 1. Schematic of a FMEJ. Plasma discharge generated by electrodes embedded along the micro-channel surface imparts momentum to the flow in the direction of the ion discharge. Positive electrodes are shown in red, negative electrodes are shown in blue and the arrow show the general direction of the incoming flow of neutral particles. Ions move from positive electrodes to negative electrodes.

II. Design Parameters

The working parameters for one embodiment of the proposed micro-thruster are given in Table 1, where the dimensions and inlet pressure were selected to obtain a Knudsen number ~ 0.1 within the transitional regime. Studying the transitional regime is of particular importance because the flow at the wall has slip condition and at low pressure the sheath/pre-sheath of the plasma will be bigger, allowing the particles to accelerate over a longer distance since most of the acceleration happens in the area of high electric field. The anode potential difference was selected to keep the power consumption below 5W. Xenon was picked as a working fluid based on how common it is as a propellant due to its high atomic mass and low ionization potential.

Table 1. Design parameters of FMEJ

Parameter	Value
Inlet Pressure	100 Pa
Length	1 cm
Height	2 mm
Working Propellant	Xenon
Potential Difference	50V

The Knudsen number is defined as the ratio of the molecular mean free path length to a representative physical length scale, which in this case is the height of the inlet of the micro-channel. The Knudsen number and mean free path are defined as[13, 17, 19]

$$Kn = \frac{\lambda}{L} \tag{1}$$

$$\lambda = \frac{1}{\sqrt{2} n \pi d^2} \tag{2}$$

The Knudsen number is used to determine which approach is more appropriate: statistical mechanics or continuum mechanics for the numerical modeling of a given flow. As Kn → 0, the flow is assumed sufficiently continuous, while for Kn > 10, the flow is assumed free-molecule. For 10^{-3} < Kn < 10 the flow is neither sufficiently continuum nor completely molecular. For this range the flow is further divided into two subcategories: slip flow regime 10^{-3} < Kn < 10^{-1} and transitional regime for 10^{-1} < Kn < 10 as explained by Raju.[12]

In this formula for mean free path, *d* is the atomic diameter of Xenon, and *n* is the neutral number density. At a pressure of 100 Pa and a working temperature of 300 K, Xenon has a mean free path of the order of 10^{-3} m. For a characteristic flow dimension of 2 mm, this gives an inlet Knudsen Number of ~ 0.1, which between the slip and the transitional flow regimes. The Knudsen number at the exit plane of the thruster is ~ 0.4.

As previously mentioned, the FMEJ devices are intended for use in microsatellites. This type of satellites have a mass typically of the order of 10kg and require small thrust at high specific impulse for attitude control and drag compensation.

Since the FMEJ micro-thruster is expected to have superior characteristics over the FMMR, the thrust and specific impulse should be comparable to FMMR designs that have been previously studied with similar geometries. A good example of FMMR characteristics is provided by Ahmed in table 2.[2] In the following table P_0 is the plenum pressure and T_w is the wall temperature of the heating chip. The heating chip is a 19.2 mm by 19.2 mm square with a thickness of 500 μm. The chip has 44 interior expansion slots, each 100 μm wide by 5.375 mm long as explain in Ref. 2. The power consumption was not provided in the study of FMMR performed by Ahmed.

Table 2.Design performance parameters of FMMR[2]

P_0 (Pa)	T_w (K)	Mass Flow Rate (kg/s)	Thrust (N)	Isp (s)
95	300	1.3343E-06	6.0446E-04	46.18
95	400	1.1502E-06	5.9265E-04	52.52
95	500	1.0299E-06	5.8689E-04	58.09
95	573	9.6222E-07	5.8319E-04	61.78

Ketsdever et al.[26] reports a propulsive efficiency of 15% for FMMR devices operating at 3.2 Watts at steady state producing a thrust of 1.7×10^{-3} N for a mass flow rate of 50 sccm and a wall temperature of 600K.

Another good comparison for FMEJ is the miniaturized 50-Watt TAL thruster (Hall Effect Thruster with Anode Layer, i.e., conductive acceleration channel walls) by Khayms[22] at MIT. This thruster has been evaluated experimentally.

Table 3. Design performance parameters of TAL[22]

	Numerical Simulation Parameters	Parameters from Experimental Test
Propellant	Xenon	-
Diameter (m)	4.8E-03	-
B-field (T)	0.5	-
Mass Flow Rate (kg/s)	1.3E-07	-
Potential Diff. (V)	300	-
Anode Current (A)	0.17	0.20
Anode Power (W)	50	60
Thrust (N)	2.2E-03	8.6E-04
I_{sp} (s)	1.6E+03	6.7E+02
Efficiency	0.32	0.048

III. Continuum Modeling of Plasma

In order to model the FMEJ several assumptions are necessary. We assumed a weakly ionized Xenon gas at low pressure and neglect the plasma interaction with the walls. Traditionally, the hydrodynamic model is considered valid only for low Knudsen numbers (0<Kn<0.1), but in recent investigations it has been shown that an accurate imposition of wall slip condition can extend the hydrodynamic model beyond the transitional flow regime.[25] Therefore the plasma is treaded as inviscid and the fluid is treated as viscous with slip boundary conditions at the wall. Two simulations are performed, a plasma simulation to calculate the body force assuming that the plasma and the gas are loosely couple and a rarefied gas simulation to obtain the thrust. The plasma simulation is explained in this section.

The continuity equations were modeled after Ref. 5. The continuity equation for electrons and ions are:

$$\frac{\partial n_i}{\partial t} + \frac{\partial n_i u_i}{\partial x} + \frac{\partial n_i v_i}{\partial y} = S \tag{3}$$

$$\frac{\partial n_e}{\partial t} + \frac{\partial n_e u_e}{\partial x} + \frac{\partial n_e v_e}{\partial y} = S \tag{4}$$

Here u and v are the velocities in the x and y directions in m/s and n is the number density in m^{-3}. The subscripts e and i stand for the electrons and ions, respectively. The term S represents the ionization rate $S_{ioniz.}$ minus the recombination rate $S_{recomb.}$

$$S = S_{ioniz.} - S_{recomb.} \tag{5}$$

$$S_{ioniz.} = \langle \sigma_i v_e \rangle n_e n_n \tag{6}$$

$$S_{recomb.} = \alpha n_e n_i \tag{7}$$

where n_e is the electron number density, n_i is the ion number density, n_n is the neutral number density, $\langle \sigma_i v_e \rangle$ is the ionization rate of Xe, σ_i is the cross section and v_e is the electron velocity.[6] α is the recombination coefficient approximated as [5, 7]

$$\alpha = 1.09 \times 10^{-20} n_e T_e^{-9/2} \tag{8}$$

In the previous formula the electron temperature is in Kelvin. The ionization rate of Xenon is given as a function of the electron temperature, T_e (eV), in Eq. (9).[6]

$$\begin{aligned} &Ionization\left(T_e < 5eV\right) \\ &\langle \sigma_i v_e \rangle \approx \langle \sigma_i \rangle \bar{v}_e = 10^{-20}\left[\left(3.97 + 0.643T_e - 0.0368T_e^{\,2}\right)\exp\left(-\frac{E_i}{T_e}\right)\right]V_{th,e} \\ &Ionization\left(T_e \geq 5eV\right) \\ &\langle \sigma_i v_e \rangle \approx \langle \sigma_i \rangle \bar{v}_e = 10^{-20}\left[-1.031\times10^{-4}T_e^{\,2} + 6.386\exp\left(-\frac{E_i}{T_e}\right)\right]V_{th,e} \end{aligned} \tag{9}$$

The previous model for the continuity equations incorporates recombination and ionization effects.[5] The neutral continuity equation is defined as:

$$\frac{\partial n_n}{\partial t}+\frac{\partial n_n u_n}{\partial x}+\frac{\partial n_n v_n}{\partial y}=-S \tag{10}$$

The ion momentum equations are[13]

$$\frac{\partial u_i}{\partial t}+u_i\frac{\partial u_i}{\partial x}+v_i\frac{\partial u_i}{\partial y}=-\frac{k_B T_i}{\mathrm{m_i n_i}}\frac{\partial n_i}{\partial x}+\left(\frac{Ze}{m_i}\right)\left(-\frac{\partial\phi}{\partial x}\right)+\left(\frac{m_e}{m_i}\right)\left(\frac{n_e}{n_i}\right)\nu_{ei}(u_e-u_i)$$
$$-\left(\frac{1}{2}\nu_{in}+\nu_c\right)(u_i-u_n)-\left(\frac{S}{n_i}\right)u_i \tag{11}$$

$$\frac{\partial v_i}{\partial t}+u_i\frac{\partial v_i}{\partial x}+v_i\frac{\partial v_i}{\partial y}=-\frac{k_B T_i}{\mathrm{m_i n_i}}\frac{\partial n_i}{\partial y}+\left(\frac{Ze}{m_i}\right)\left(-\frac{\partial\phi}{\partial y}\right)+\left(\frac{m_e}{m_i}\right)\left(\frac{n_e}{n_i}\right)\nu_{ei}(v_e-v_i)$$
$$-\left(\frac{1}{2}\nu_{in}+\nu_c\right)(v_i-v_n)-\left(\frac{S}{n_i}\right)v_i \tag{12}$$

T_i is the temperature of the ions in electron volts, which is assumed to remain constant. The electric potential, ϕ, is in volts. The charge state, Z, is assumed to be 1 for the given case which corresponds to single charge ions. ν_c is the ion charge exchange frequency, ν_{ei} is the electron ion collision frequency, and ν_{in} is the ion neutral collision frequency. The values for the respective collision frequencies are calculated for Xe gas as shown in Ref. 5 and Ref. 8. The factor of ½ before the ion-neutral collision term comes from reduced mass approximation, $[m_i m_n/(m_n+m_i)] \approx m_i/2$ where m_n is the mass of a neutral atom and m_i is the mass of an ion.[5]

Similarly the electron momentum equations are[13]

$$\frac{\partial u_e}{\partial t}+u_e\frac{\partial u_e}{\partial x}+v_e\frac{\partial u_e}{\partial y}=-\frac{k_B T_e}{\mathrm{m_e n_e}}\frac{\partial n_e}{\partial x}-\frac{k_B}{m_e}\frac{\partial T_e}{\partial x}-\left(\frac{e}{m_e}\right)\left(-\frac{\partial\phi}{\partial x}\right)-\nu_{ei}(u_e-u_i)-\nu_{en}(u_e-u_n)$$
$$-\left(\frac{S}{n_e}\right)u_e \tag{13}$$

$$\frac{\partial v_e}{\partial t}+u_e\frac{\partial v_e}{\partial x}+v_e\frac{\partial v_e}{\partial y}=-\frac{k_B T_e}{\mathrm{m_e n_e}}\frac{\partial n_e}{\partial y}-\frac{k_B}{m_e}\frac{\partial T_e}{\partial y}-\left(\frac{e}{m_e}\right)\left(-\frac{\partial\phi}{\partial y}\right)-\nu_{ei}(v_e-v_i)-\nu_{en}(v_e-v_n)$$
$$-\left(\frac{S}{n_e}\right)v_e \tag{14}$$

where ν_{en} is the electron neutral collision frequency calculated as in Ref. 5.

A number of physical parameters are necessary to calculate the momentum of the charge particles in Eqs. (11-14). These parameters below represent the *thermal velocity of electrons*, *Bohm velocity* (V_B), *electron-neutral frequency of collisions*, *electron-ion frequency of collisions*, *ion-neutral frequency of collisions*, and *charge exchange frequency*, respectively. Where all units are in SI except T_e which is in eV.

$$V_{th,e}=\left(\frac{8k_B T_e}{\pi m_e}\right)^{1/2} \tag{15}$$

$$V_b = \left(\frac{k_B T_e}{m_i} \right)^{1/2} \tag{16}$$

$$\nu_{en} = n_n \left(27.0 \times 10^{-20} \right) V_{th,e} \tag{17}$$

$$\nu_{ei} = 5.0 \times 10^{-20} \left(1.0 + \frac{\left(T_e E_i \right)}{\left(T_e + E_i \right)^2} \right) \exp\left(-\frac{Ei}{T_e} \right) V_{th,e} n_n \tag{18}$$

$$\nu_{in} = \nu_{en} \sqrt{\frac{m_e}{m_i}} \tag{19}$$

$$\nu_c = n_n \cdot 1.0 \times 10^{-20} V_b \tag{20}$$

$$\nu_c = n_n \cdot 1.0 \times 10^{-20} V_b \tag{21}$$

Neglecting the effect of radiation, viscous dissipation, and the thermal conduction the electron energy equation is defined as: [9, 13, 23]

$$\begin{aligned} &\frac{3}{2}\left[\frac{\partial \left(k_B T_e \right)}{\partial t} + u_e \frac{\partial \left(k_B T_e \right)}{\partial x} + v_e \frac{\partial \left(k_B T_e \right)}{\partial y} \right] + k_B T_e \left[\frac{\partial u_e}{\partial x} + \frac{\partial v_e}{\partial y} \right] = m_e \nu_{ei} \left[\begin{array}{l} \left(u_i - u_e \right)^2 + \left(v_i - v_e \right)^2 \\ +3 \dfrac{k_B}{m_i} \left(T_i - T_e \right) \end{array} \right] \\ &+ m_e \nu_{en} \left[\begin{array}{l} \left(u_n - u_e \right)^2 + \left(v_n - v_e \right)^2 \\ +3 \dfrac{k_B}{m_n} \left(T_n - T_e \right) \end{array} \right] - k_B \left[\frac{3}{2} T_e + \varphi E_i - \frac{m_e}{2} \left(u_e^2 + v_e^2 \right) \right] \frac{S}{n_e} \end{aligned} \tag{22}$$

In the previous equation, the directed kinetic energy term, $\frac{m_e}{2}\left(\vec{V}_e^{\,2}\right)$, is assumed to be smaller than the random kinetic energy term and is neglected. The term, φE_i, represents losses due to ionization,[9] where E_i is the first ionization of Xenon, φ is the normalized ion production cost. The normalized ion production cost can be approximated by a function with coefficients A=0.254, B=0.677, and C=2.00 for Xenon using the following equation where z is the dimensionless electron kinetic temperature .[9]

$$\varphi = A \exp\left(\frac{B}{z} \right) + C \tag{23}$$

$$z = \frac{k_B T_e}{E_i}$$

Finally the Poisson's equation is used to calculate the electric potential

$$-\left(\frac{\partial}{\partial x}\left(\frac{\partial \varepsilon \phi}{\partial x} \right) + \frac{\partial}{\partial y}\left(\frac{\partial \varepsilon \phi}{\partial y} \right) \right) = e\left(Z n_i - n_e \right) \tag{24}$$

where ϕ is the potential, e is the electron charge, and ε is the permittivity.

It is important to note that for this case the neutral velocity is assumed to be constant and its component in the y direction is zero. The temperature of ions is assumed to be in thermal equilibrium with the neutral atoms at T_i=300K.

The following parameters are used to non-dimensionalize the previous equations. These are the reference velocity of ions and neutrals, velocity of electrons, number density of ions and electrons, number density of neutrals,

collision frequency, electron temperature, electric potential, length scale, and time scale. C is a constant that is picked to obtain a desire length scale.

$$V_{ref,i,n} = \left(\frac{k_B E_i}{m_i} \right)^{1/2} \qquad T_{ref} = E_i = 12.1eV$$

$$V_{ref,e} = \left(\frac{k_B E_i}{m_e} \right)^{1/2} \qquad e\phi_{ref} = k_B E_i$$

$$n_{ref,e,i} = 1.0 \times 10^{20} \qquad l_0 = \frac{V_{ref}}{\nu_{ref}} = 0.01m \tag{25}$$

$$n_{ref,n} = 1.0 \times 10^{22} \qquad t_0 = \nu_{ref}^{-1}$$

$$\nu_{ref} = C\sigma_{ref} n_{ref} V_{ref}$$

$$= C\left[\left(3.6 \times 10^{-20} m^2 \right) \sqrt{m_i / m_e} \right] n_{ref,e,i} V_{ref,i,n}$$

IV. Finite Element Based Modeling Element Based Multiscale Ionized Gas (MIG) Flow Code

The finite element method has been used since the 1950's in the field of structural analysis, but after the development of weighted residual criteria to increase stability, it is now commonly use as a numerical method in the field of heat transfer and fluid mechanics.[4] The finite element method creates a solutions approximation as a series of known spatial functions multiplied by a set of unknown expansion coefficients. In this case we make use of the Galerkin weak statement method, where the solution is approximated as a power series

$$L(q) = \sum a_i \phi_i \left(x_j \right) \tag{27}$$

where a_i are unknown coefficients and $\phi_i(x_j)$ are known functions of x_j.[3]

The term "weak statement" of the Galerkin method originates from the integration by parts and Stoke's theorem by which the differentiability requirement for the approximation is weakened by one order.

The numerical modeling of the system of equations shown in this paper is achieved through the use of a multivariable design code developed by Roy et al.[10, 11] Using L as a differential operator, a general formulation for Eqs.(3-4, 10-14, 22, 24) can be expressed as L(U)=0, where $U=\{n_i, n_e, n_n, u_i, v_i, u_e, v_e, T_e, \phi\}^T$ [8]. The code has since been successfully employed for a class of plasma and flow related problems.[4, 5, 24]

The final element based modeling element based multiscale ionized (MIG) gas flow code was combined with an artificial diffusion method, called non-linear Sub-Grid eMbedded (SGM) nonhierarchical finite element bases, in order to provide stability to the simulation. The implementation of such method has been previously described by the references provided.[14, 15]

V. Boundary Conditions of Plasma Simulation

The boundary conditions implemented assume no penetration of ions and electrons at the walls, $v_i=v_e=0$. At the inlet, the number density of neutrals is constant, and there is no penetration of ions and electrons, ($n_n=2.4x10^{22}$ and $u_i=u_e=0$). Constant neutral velocity is assumed throughout the domain, $u_n=100$m/s and $v_n=0$ m/s. In this case the T_i and T_n, which are ion and neutral temperatures, are assumed to be constant and have the same temperature as the incoming gas ~300K. At the outlet, it is assumed that no electrons come from the plume, ($u_e=0$), since the plume will have only neutral particles.

At the cathode (negative electrode), the boundary conditions assume constant electron temperature of T_e = 2 eV, thermal velocity of electrons traveling out of the electrode, a fixed number density of electrons of the order of the expected secondary electron emission, ($n_e \sim (0.05 n_i v_i / v_e)_{Cathode}$), and 0 electric potential. At the anode (positive

electrode) the boundary conditions assume no penetration of the ions, (v_i=0), and an electric potential of 50 V. The rest of the boundary conditions needed are zero flux normal to the edges of the domain (d/dx=0 or d/dy=0).

VI. Results of Plasma Simulation

The code provides data about number densities of ions, electrons, and neutrals, velocity components in 2-D of ions and electrons and electron temperature. Also the electric potential distribution is calculated.

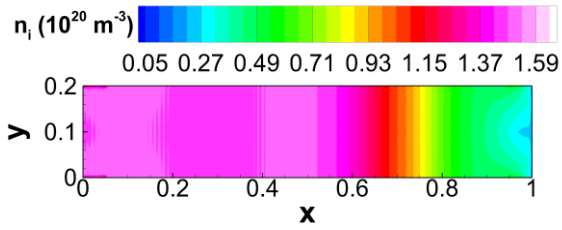

Figure 2a. Ion number density.

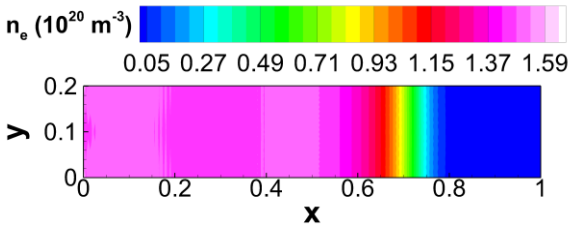

Figure 2b. Electron number density.

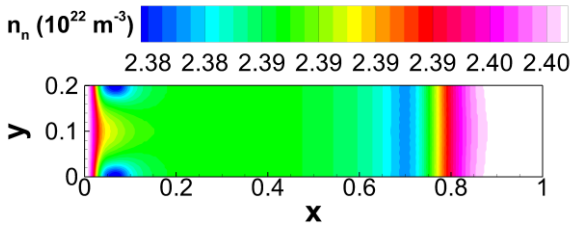

Figure 2c. Neutral number density.

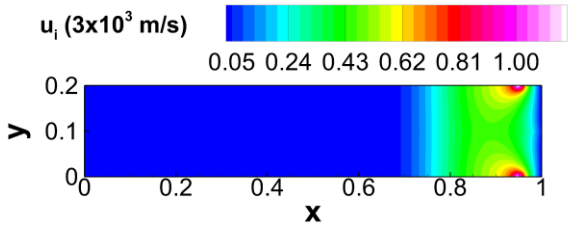

Figure 2d. Ion velocity u_i.

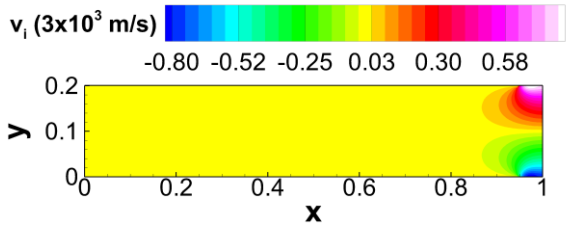

Figure 2e. Ion velocity v_i.

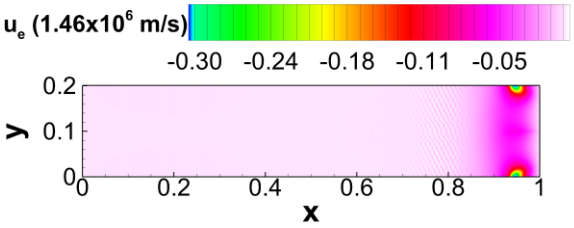

Figure 2f. Electron velocity u_e.

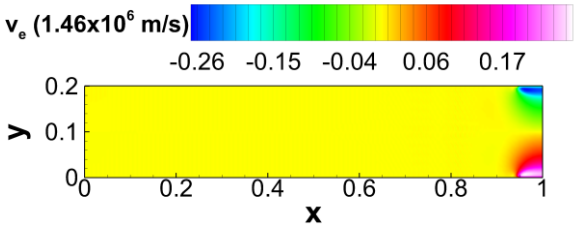

Figure 2g. Electron velocity v_e.

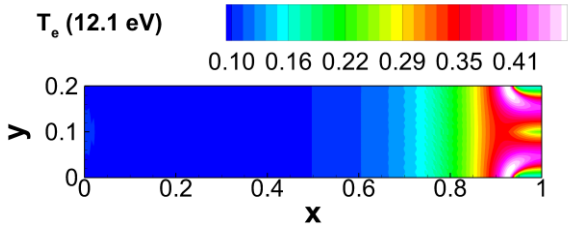

Figure 2h. Electron temperature.

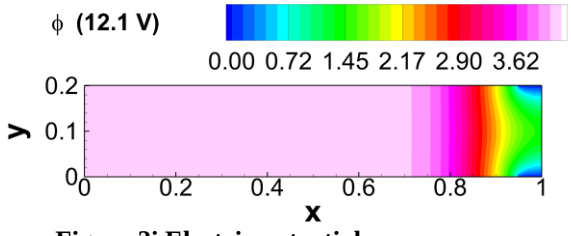

Figure 2i.Electric potential.

In fig. 2a the ion number density can be observed increasing away from the inlet only to decrease again near the outlet due to an increase in ion velocity and an increase in recombination at the Cathode. The maximum ion number density is attained upstream of the acceleration region. In fig. 2b, the electron number density is shown. The electron number density in most of the region between 0 and 0.6 cm is of the same order of ion number density in the quasi-neutral region. The electron number density decreases at the outlet due to high electron velocity near the Cathode. The rapid increase in the ion number density is reflected in the rapid decrease in the neutral number density in fig. 2c. This is consistent with the fact that as the neutrals enter the thruster chamber they undergo impact ionization. The neutral number density decreases due to ionization at the inlet and increases near the outlet to similar values as those at the inlet due to recombination of the ions at the Cathode. In figs. 2d through 2g the velocity components in 2D of ions and electrons are shown, in these plots the acceleration region can be observed near the Cathode where the maximum electric field is located as expected. Figure 2h shows the electron temperature, which increases away from the Cathode as the fast moving electrons from the Cathode slow down due to collisions with heavy particles and decrease to a near constant value in the ionization region where the channel have quasi-neutrality and higher ionization. The electron temperature is expected to increase due to Ohmic heating, near the cathode and decrease at the edge where the quasi-neutral region meets the acceleration region due to high ionization. The final plot, in fig. 2i, shows the electric potential.

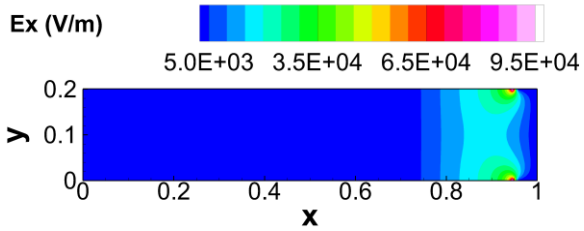

Figure 3a. Electric Field Ex=-dϕ/dx.

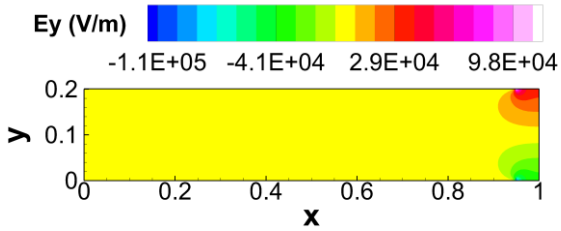

Figure 3b. Electric Field Ey=-dϕ/dy.

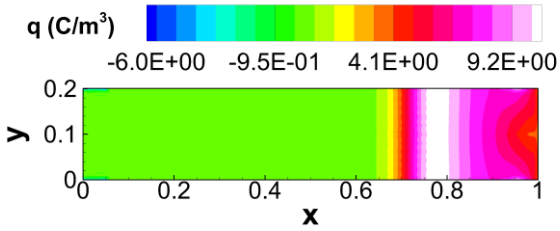

Figure 3c. Charge density $q=e(n_i-n_e)$.

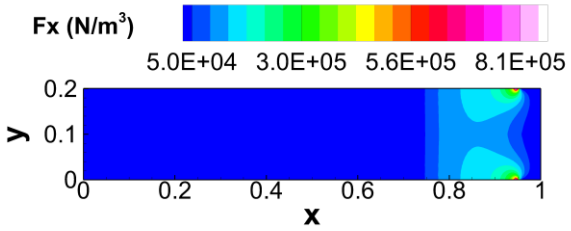

Figure 3d. Body Force $F_x=qE_x$.

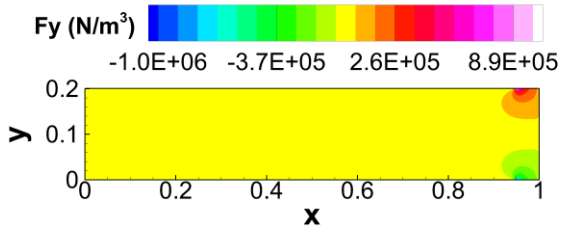

Figure 3e. Body Force $F_y=qE_y$.

In the following figures the electric field components, charge density, and body force components are shown. The body force components are needed to run a fluid simulation since the device will create thrust by impinging a force on the fluid.

The anode current and the anode power can be calculated from this data as well as the total body force over the entire volume for this particular micro-thruster. It is important to point out that the actuators themselves will not produce any thrust from charge particles since all the ions recombine at the cathode. The thrust in this device is

created by the body force on the fluid and the body force is expected to remain relatively constant regardless of the changes in the velocity of the neutrals and number density of the neutrals as long as both of these values remain within the same order of magnitude.

Table 4.Performance parameters of FMEJ

	Design
Propellant	Xenon
Height (m)	2.0E-03
Length (m)	1.0E-02
B-field (T)	0
Potential Diff. (V)	50
Anode Current (A)	2.324292E-02
Anode Power (W)	1.161518E+00
Total body Force (x-comp) (N)	1.185709E-03

VII. Continuum Modeling of a Rarified Gas Simulation with Plasma Body Force

The previous data of the body force components was used to run a fluid simulation for rarefied Xenon gas. In the following simulation, the same finite element program and artificial diffusion method were used as the one in our plasma model. Compressible flow equations were used in this simulation with the assumption of ideal gas, instead of those describing the plasma.[12]

Continuity equation,

$$\frac{\partial \rho}{\partial t}+\frac{\partial (u\rho)}{\partial x}+\frac{\partial (v\rho)}{\partial y}=0 \tag{30}$$

Momentum equations in 2D,

$$\frac{\partial u}{\partial t}+u\frac{\partial u}{\partial x}+v\frac{\partial u}{\partial y}+R\frac{\partial T}{\partial x}+\frac{RT}{\rho}\frac{\partial \rho}{\partial x}-\frac{\mu}{\rho}\left[\frac{4}{3}\frac{\partial^2 u}{\partial x^2}+\frac{\partial^2 u}{\partial y^2}+\frac{1}{3}\frac{\partial^2 v}{\partial x \partial y}\right]-\frac{F_x}{\rho}=0 \tag{31}$$

$$\frac{\partial v}{\partial t}+u\frac{\partial v}{\partial x}+v\frac{\partial v}{\partial y}+R\frac{\partial T}{\partial y}+\frac{RT}{\rho}\frac{\partial \rho}{\partial y}-\frac{\mu}{\rho}\left[\frac{\partial^2 v}{\partial x^2}+\frac{4}{3}\frac{\partial^2 v}{\partial y^2}+\frac{1}{3}\frac{\partial^2 u}{\partial x \partial y}\right]-\frac{F_y}{\rho}=0 \tag{32}$$

Energy equation,

$$\begin{aligned}&\rho C_v\left[\frac{\partial T}{\partial t}+u\frac{\partial T}{\partial x}+v\frac{\partial T}{\partial y}\right]+\rho RT\left[\frac{\partial u}{\partial x}+\frac{\partial v}{\partial y}\right]-\frac{\partial}{\partial x}\left(\kappa\frac{\partial T}{\partial x}\right)-\frac{\partial}{\partial y}\left(\kappa\frac{\partial T}{\partial y}\right)\\&-\mu\left[\frac{4}{3}\left(\frac{\partial u}{\partial x}\right)^2+\frac{4}{3}\left(\frac{\partial v}{\partial y}\right)^2-\frac{4}{3}\frac{\partial u}{\partial x}\frac{\partial v}{\partial y}+\left(\frac{\partial v}{\partial x}\right)^2+\left(\frac{\partial u}{\partial y}\right)^2+2\frac{\partial v}{\partial x}\frac{\partial u}{\partial y}\right]=0\end{aligned} \tag{33}$$

In these equations, ρ is the density, u and v are the x and y components of velocity, T is the gas temperature, R is the gas constant, R=63.33 J/(kg K), C_v is the specific heat at constant volume, C_v=91.53 J/(kg K), κ is the thermal conductivity, κ=5.192E-03 W/(m K), and μ is the viscosity, μ= 2.11E-05 Pa·s. The previous constants are for Xenon at 300K.

VIII. Boundary Conditions for Rarefied Gas Simulation

The boundary conditions for the following rarefied gas simulation with a plasma body force are: fixed density, temperature and y-component of velocity at the inlet, ρ=P/RT, T=300K, v=0 m/s, where inlet pressure is P=100Pa. At the walls there is no penetration, v=0. At the outlet, temperature is calculated to satisfied an outlet pressure, T=P/Rρ for an outlet pressure of P=100Pa while ρ is calculated by the program. Boundary conditions for a rarefied gas are used for variables u and T at the wall.[12, 20, 21]

$$u_{gas} - u_{wall} = \frac{2-\sigma_v}{\sigma_v}\lambda\left(\frac{\partial u}{\partial y}\right)_w + \frac{3}{4}\frac{\mu}{\rho T_{gas}}\left(\frac{\partial T}{\partial x}\right)_w \tag{34}$$

$$T_{gas} - T_{wall} = \frac{2-\sigma_T}{\sigma_T}\left[\frac{2\gamma}{\gamma+1}\right]\frac{\lambda}{\mathrm{Pr}}\left(\frac{\partial T}{\partial y}\right)_w \tag{35}$$

In these equations the new variables introduced are the Prandtl number, $\mathrm{Pr}=C_p\mu/\kappa$, the specific heat ratio, $\gamma=C_p/C_v$ where C_p is the specific heat at constant pressure, the tangential momentum accommodation coefficient, σ_v ($0\le\sigma_v\le1$), and the thermal accommodation coefficient, σ_T ($0\le\sigma_T\le1$), at the walls. *Specular* reflection happens when the gas molecules are reflected from the wall at an angle equal to the incident angle exerting no shear stress on the wall. *Diffuse* reflection happens when the channel surface is rough and the gas molecules are reflected at random angles. The accommodation coefficients indicate the fraction of the molecules reflected diffusively from the walls.[12] For this case the accommodation coefficients were assumed to be equal to one corresponding with *diffuse* reflection since the surface roughness of the channel is unknown ($\sigma_v=1$, $\sigma_T=1$).

Using the definition of mean free path given previously in Eq. (2) and the expression for the viscosity of dilute gases, shown below in Eq.(36), obtained by the Chapman-Enskog method where m is the molecular mass and *a* is the atomic radius, the boundary condition formulas can be modified.[19]

$$\mu = \frac{5}{64a^2}\left(\frac{mk_BT}{\pi}\right)^{1/2} \tag{36}$$

The boundary conditions can be solved for the fluxes where $T_{wall}=300K$ and $u_{wall}=0$.[12]

$$\mu\left(\frac{\partial u}{\partial y}\right)_w = \frac{5\rho\sqrt{2\pi RT}}{16}\frac{\sigma_v}{(2-\sigma_v)}\left[u_{gas} - u_{wall} - \frac{3}{4}\frac{\mu}{\rho T_{gas}}\left(\frac{\partial T}{\partial x}\right)_w\right] \tag{37}$$

$$\kappa\left(\frac{\partial T}{\partial y}\right)_w = \frac{5\rho\sqrt{2\pi RT}}{16}\frac{\sigma_v}{(2-\sigma_v)}\left[\frac{\gamma+1}{2}\right]C_v\left[T_{gas} - T_{wall}\right] \tag{38}$$

Solving the equations in term of the fluxes allows the boundary conditions to be implemented into the simulation through the weak statement of the Galerkin Method. The rest of the boundary conditions needed are zero flux normal to the edges of the domain (d/dx=0 or d/dy=0).

IX. Results of Rarefied Gas Simulation

The code provides information about the density, velocity components in 2D, and Temperature. Pressure can be obtained by post-processing the data using the ideal gas law.

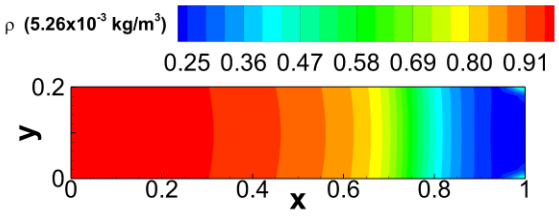

Figure 4a. Density of gas.

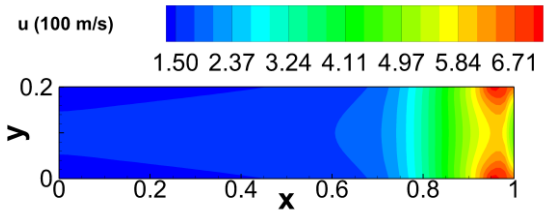

Figure 4b. Velocity of gas, u.

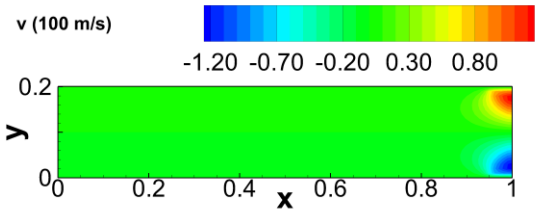

Figure 4c. Velocity of gas, v.

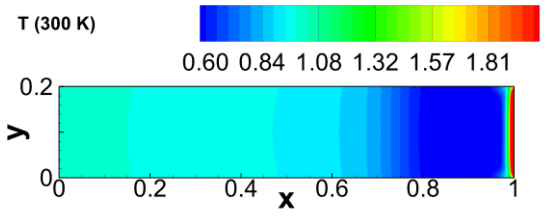

Figure 4d. Temperature of gas.

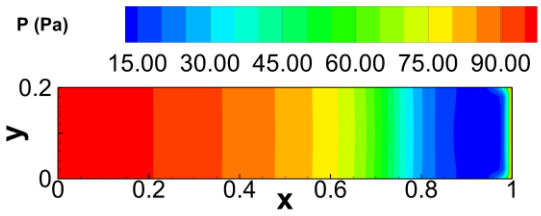

Figure 4e. Pressure of gas.

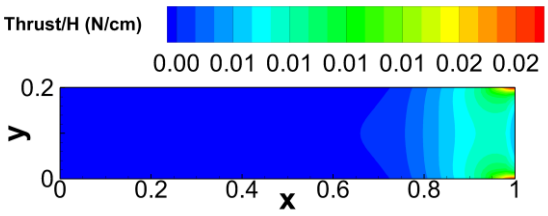

Figure 4f. Thrust per unit of height.

In the previous figures the density, velocity components, temperature, pressure of the gas, and thrust per unit of height of the exit are shown. In fig. 4a the density decreases as it gets close to the exit due to the increase in velocity and it has local maxima at the edge of the walls of the channel at the exit plane due to the impingement of the force toward the wall. The velocity components in fig. 4b and fig. 4c behave in accordance with the force distribution shown in the plasma simulation with the greatest magnitude near the exit. The temperature plot in fig. 4d has a spike at the exit plane due to the particles deceleration since the x-component of the body force decreases to near zero magnitude at the exit plane. Figures 4e and 4f are in accordance with expected behavior.

After observing our results, it is obvious that the velocity of the gas, the neutral particles in the plasma simulation, is going to remain of the order of ~10^2 m/s which is well below the Bohm velocity which is of the order of ~10^3 m/s and our number density of neutrals at the minimum value is of the order of 10^{21} m^{-3} which is high enough to slow down the electrons through collisions. Lower values of neutral number density would allow the electrons to travel faster, increasing the current through the system and the power consumed.

In order to calculate the performance of the micro-thruster the mass flow rate, thrust, specific impulse, and efficiency are calculated using the following formulas.[6, 16, 18]

$$\dot{m} = A_e\left[m_i\left(n_i u_i + n_n u_n\right) + m_e\left(n_e u_e\right)\right] \tag{39}$$

$$F_{thrust} = m_i A_e\left(n_i u_i^{\,2} + n_n u_n^{\,2}\right) + m_e A_e\left(n_e u_e^{\,2}\right) + \left(p_e - p_\infty\right) \tag{40}$$

$$I_{sp} = \frac{F_{thrust}}{A_e\left[m_i\left(n_i u_i + n_n u_n\right) + m_e\left(n_e u_e\right)\right] g_0} \tag{41}$$

$$\eta = \frac{\left(F_{thrust}\right)^2}{2\dot{m}P_{in}}$$

where m_i and m_e are the masses of an ion and electron respectively. Ions and neutrals are expected to have equal masses. A_e is the cross-sectional area at the exit. p_e and p_∞ are the pressures at the exit and infinity, g_0 is the gravitational constant, and P_{in} is the electrical power input.

Since no electrons are expected to leave the domain and all ions are expected to recombine at the Cathode, only the neutral particles produce thrust. The pressure at the exit plane is expected to be the same as at infinity and the previous equations simplify to the following ones.

$$\dot{m} = m_n n_n u_n A_e = \left(\rho u\right)_{gas} A_e \tag{42}$$

$$F_{thrust} = m_n n_n u_n^{\,2} A_e = \left(\rho u^2\right)_{gas} A_e \tag{43}$$

$$I_{sp} = \frac{F_{thrust}}{\dot{m} g_0} \tag{44}$$

$$\eta = \frac{\left(F_{thrust}\right)^2}{2\dot{m}P_{in}} \tag{45}$$

After integrating the appropriate variables over the height of the channel the following results were obtained.

Table 5.Design performance parameters of FMEJ

Mass Flow Rate (kg/s)	3.099704E-06
Thrust (N)	1.702494E-03
I_{sp} (s)	5.598818E+01
Efficiency	0.402530E+00

As explained in Section VII the inlet density of the gas is fixed, this value is the same as the one in the plasma simulation. The rarefied gas simulation calculates the inlet velocity since the inlet velocity of the gas will depend on the pressure difference, the plasma body force, and the interaction of the gas with the walls. Due to the fact that the x-component of velocity of the gas is calculated by the rarefied gas code instead of being fixed, the mass flow rate will deviate from the plasma simulation. The change in mass flow rate is not expected to change the plasma force since the change in mass flow rate is due to a change in the velocity of the gas, which is the velocity of the neutrals in the plasma simulation, and not due to a change in the neutral number density. The body force is expected to remain the same as long as the neutral velocity does not increase to higher orders of magnitude than originally predicted conserving the assumption that the plasma is loosely couple with the fluid simulation. The thrust is of the order of milli-Newtons similarly to the 50-Watt TAL thruster previously mentioned in the introduction in Table 3,[22] while the specific impulse is similar to the specific impulse for FMMR in Table 2.[2] It is important to note that an accurate comparison between FMMR and FMEJ cannot be done at this time since the same channel geometry, pressure difference between inlet and outlet, and power would be needed for both in order to compare them effectively, but it seems that FMEJ is able to achieve similar thrust to FMMR at a higher efficiency after comparing the data from Ref. 26.

Table 6. Comparison between HET, FMMR, and FMEJ

	HET[22]	**FMMR[26]**	**FMEJ**
Mass Flow Rate (kg/s)	1.3E-07	3.0E-06	3.099704E-06
Power (W)	50	3.2	1.161518E+00
Thrust (N)	2.2E-03	1.7E-03	1.702494E-03
I_{sp} (s)	1.6E+03	5.8E+01	5.598818E+01
Efficiency	0.32	0.15	0.40253

X. Conclusion

As formation flying of the micro-scale commercial and military spacecrafts become more frequent, and frequent exploration of other planets such as Mars becomes more feasible, scientist are researching for ways to decrease the power budget of launching satellites into space. The new class of micro-thruster, FMEJ, introduced here shows promise. The numerical result predicts an efficiency greater than 40% which is similar to many other electric propulsion devices such as hall thrusters while showing equal thrust to FMMR devices shown in Ref.26 at higher efficiency. The results show that FMEJ is a viable and novel type of electric propulsion that should be investigated further and if possible optimize. Further numerical investigation is needed to optimize the design. There may be some advantages in using different configurations of the electrodes as well as variable area along the channel. Insulating the thruster instead of assuming that it has isothermal walls may also help improve the energy budget, and hence, the efficiency. It may also increase the thrust while decreasing the mass flow rate which may help improve the specific impulse. There are obvious tradeoffs with the proposed changes to the numerical simulation, but the idea is to test as many configurations and parameters as possible in order to develop a robust design. To better assess the performance of FMEJ efforts are underway to test the micro-thruster experimentally by the Applied Physics Research Group at the University of Florida.

References

[1]S. Roy, 2009, "Method and Apparatus for Small Sat. Propulsion," UF Patent Application 61/304,915, WO/2011/103194A2 published on 25 August 2011

[2]Z. Ahmed, S.F. Gimelshein, "Numerical Analysis of Free Molecule Micro-Resistojet Performance," 41st AIAA/ASME/ SAE/ASEE Joint Propulsion Conference & Exhibit, Jul 2005, Tucson, Arizona, pp 1-11.

[3]T. Deconinck, S. Mahadevan, and L. L. Raja, "Simulation of Direct-Current Microdischarge for Micro Plasma Thruster," IEEE Transactions on Plasma Science, Vol.36, Num.4, 2008, pp 1200-1201.

[4]S. Roy, R. Raju, H.F. Chuang, B.A. Cruden, and M. Meyyappan, "Modeling gas flow through microchannels and nanopores," Journal of Applied Physics, Vol. 93, Num.8, 2003, pp. 4870-4879.

[5]S. Roy and B.P. Pandey, "Modeling low pressure collisional plasma sheath with space-charge effect," *Physics of Plasma*, Vol.10, Num.6, 2003, pp. 2578- 2585.

[6]D.M. Goebel, and I. Katz, "Fundamentals of Electric Propulsion: Ion and Hall Thrusters," Jet Propulsion Lab., California Institute of Technology, March 2008, pp. 475.

[7] M. Mitchner and C.H. Kruger, *Partially Ionized Gases*, Wiley-Interscience, New York, 1973.

[8]S. Roy and B.P. Pandey, "Development of a Finite Element-Based Hall-Thruster Model," Journal of Propulsion and Power, Vol.19, Num.5, 2003, pp. 964- 967.

[9]J. M. Fife, "Two-Dimensional Hybrid Particle-In-Cell Modeling of Hall Thruster," Master of Science Dissertation, Aeronautics and Astronautics Dept., Massachusetts Institute of Tech., MA, 1983.

[10]S. Roy, "Combining Galerkin Matrix Perturbation with Taylor Weak Statement Algorithms," Computer Method in Applied Mechanics and Engineering, Vol.184, Num.1-2, 2000, pp.87-98.

[11]D. Balagangadhar, and S. Roy, "Design Sensitivity Analysis and Optimization of Steady Fluid-Thermal Systems," Computer Methods in Applied Mechanics and Engineering, Vol.190, Num.42, 2001, pp 5465-5479; also "Erratum," Vol.191, Num.3-5, pp.509, 510.

[12]R. Raju, "Hydrodynamic Model for Investigation of Gas Flows Through Micro-Geometries and Nanopores," M.S. Dissertation, Mechanical Engineer Dept, Kettering University, Flint, MI, 2003.

[13]J.D. Huba, "NRL Plasma Formulary," Beam Physics Branch, Plasma Physics Division, Naval Research Lab, Washington, DC, 2009.

[14]S. Roy, and M. Fleming, "Nonlinear sub-grid embedded element-free Galerkin method for monotone CFD solutions," ASME Cd-Rom, 1999, pp. 1-7.

[15]S. Roy, and A.J. Baker, "Sub Grid eMbedding (SGM) Algorithm – Part II, Navier-Stokes solutions," Journal of Numerical Heat Transfer –Part B (Fundamentals), Vol.33, Num.1, 1998, pp. 5-36.

[16]E. Ahedo, C. Martinez, and S. Martinez, "One dimensional model of the plasma flow in a Hall thruster," Physics of Plasma, Vol.8, Num.6, 2001, pp. 3058-3068.

[17]R.J. Goldston, and P.H. Rutherford, *Introduction to Plasma Physics*, Plasma Physics Lab., Princeton University, Institute of Physics Publishing, Bristol and Phyladelphia, 1995, pp. 150.

[18]P. Hill, and C. Peterson, *Mechanics and Thermodynamics of Propulsion*, 2nd ed., Addison-Wesley Publishing Company, Inc, Reading, Massachusetts, 1992, pp. 656.

[19]A.R. Choudhuri, *The Physics of Fluids and Plasmas: an Introduction for Astrophysicists*, Cambridge University, Cambridge University Press, Cambridge, United Kingdom,1998, pp. 19.

[20]J.C. Maxwell, "On Stresses in Rarefied Gases Arising from Inequalities of Temperature," Philosophical Transactions of the Royal Society Part1, Vol.170, 1879, pp. 231-256.

[21]von M. Smoluchowski, "Ueber wärmeleitung in verdünnten gasen," Annalen der Physik und Chemi, Vol. 64, 1898, pp. 101-130.

[22]J.J. Szabo, Jr., "Fully Kinetic Numerical Modeling of a Plasma Thruster," PhD Dissertation, Aeronautics and Astronautics Dept, Massachusetts Institute of Technology, Cambridge, MA, 2001.

[23]J.A. Bittencourt, *Fundamentals of Plasma Physics*, Pergamon Press, New York, 1986, pp. 212-213.

[24]S. Roy, and B.P. Pandey, "Numerical Investigation of a Hall Thruster Plasma," Physics of Plasma, Vol.9, Num.9, 2002, pp. 4052-4060.

[25]S. Roy, S.M. Cooper, M. Meyyappan, and B.A. Cruden, "Single component gas transport through 10nm pores: Experimental data and hydrodynamic prediciton," Journal of Membrane Science, Vol.253, 2005, pp. 209-215.

[26]A.D. Ketsdever, R.H. Lee, and T.C. Lilly, "Performance testing of a micro-fabricated propulsion system for nanosatellite applications," Journal of Micromechanics and Microengineering, Vol.15, 2005, pp. 2254-2263.